Heterometallic Complexes

DOI: 10.1002/anie.201007872

Tuning the Spin State of Cobalt in a Co–La Heterometallic Complex through Controllable Coordination Sphere of La**

Song-Song Bao, Yi Liao, Yan-Hui Su, Xu Liang, Feng-Chun Hu, Zhihu Sun, Li-Min Zheng, Shiqiang Wei,* Roger Alberto, Yi-Zhi Li, and Jing Ma**

Paramagnetic molecular materials with electronic structures sensitive to the environment are very attractive owing to potential applications in molecular devices and sensors.[1] Great efforts have been made in synthesizing bistable paramagnetic molecules or polymers that exist in two different spin states, which can be tuned by an external stimulus such as temperature, pressure, or light.[2–4] Cobalt ions can exist in multiple oxidation states, and hence are good candidates for construction of molecular materials that can switch between two different oxidation states, typically between Co^{III} and Co^{II}. A number of cobalt semiquinonate complexes undergo valence transition in response to external stimuli such as temperature and light (valence tautomerism).[5,6] In a few bimetallic compounds, such as Co–Fe(Os) cyanometalates, thermally induced charge transfer occurs between the two redox-active metal ions.[7] The shift of the equilibrium between Co^{III} and Co^{II} is accompanied by a drastic change in their magnetic and optical properties. As far as we are aware, valence changes in cobalt coordination polymers induced by a second metal coordination sphere have never been described in the literature.

Here we present a novel approach to manipulate the oxidation state of cobalt by a controllable second metal coordination sphere. Polytopic ligand 1,4,7-triazacyclononane-1,4,7-triyl-tris(methylenephosphonic acid) ($notpH_6$) was utilized to generate an octahedral $Co^{III}(notp)^{3-}$ unit with linkages to $La(H_2O)_4^{3+}$ through phosphonate oxygen atoms, forming a heterometallic polymer [ls-$Co^{III}La^{III}$(notp)-$(H_2O)_4$]·n H_2O (**1a**), in which the Co^{III} ion is in a diamagnetic low-spin (ls) state. Gradual removal of the aqua ligands of the Ln^{III} ion, which depends on the dehydration temperature, has a remarkable impact on the spin state of cobalt.

Compound **1a** is a rare example of metal phosphonates with both 3d and 4f metal ions.[8] It crystallizes in monoclinic space group $P2_1/c$.[9] The octahedral Co^{III} ion is surrounded by three phosphonate oxygen atoms (O2, O5, and O8) and three nitrogen atoms (N1, N2, and N3) from the same $notp^{6-}$ ligand in a mononuclear $Co^{III}(notp)^{3-}$ unit (Co–O 1.923(3)–1.934(3), Co–N: 1.931(4)–1.940(4) Å). This unit behaves as a tetradentate "ligand" and links to four La^{III} ions through phosphonate oxygen atoms O1, O3, O4, and O7 to form a two-dimensional waved layer containing six- and eight-membered rings. Each La atom is coordinated by eight oxygen atoms, four of which are phosphonate oxygen atoms from four $Co(notp)^{3-}$ units, and the remainder oxygen atoms of water molecules. The interlayer space is filled by the lattice water molecules with extensive hydrogen-bonding interactions (Figure 1a and b). Thermal analysis and XRD measurements confirm that both the coordinated and lattice water molecules can be removed on heating to 220 °C with retention of the network structure. The fully dehydrated sample H[hs-$Co^{II}La^{III}$(notp)] (**1a-220**) can be redissolved in water, from which crystalline **1a** can be obtained within one day in the presence of oxygen (Supporting Information).

Magnetic susceptibilities, measured in the temperature range 1.8–300 K under an external field of 2 kOe (Figure 1c), reveal a diamagnetic nature for compound **1a**, in agreement with the presence of a low-spin Co^{III} (μ_{eff}/Co(300 K) = 0 μ_B). After heating **1a** at 120 °C for 1 h, the resulting sample **1a-120** becomes paramagnetic. The paramagnetic behavior becomes more significant if **1a** is heated at a higher temperature. Assuming a g value of 2.0, the room-temperature effective magnetic moments μ_{eff}/Co(300 K) are 0.48 μ_B for **1a-120**, 0.91 μ_B for **1a-140**, 1.98 μ_B for **1a-160**, 2.49 μ_B for **1a-180**, 4.15 μ_B for **1a-220**, and 4.35 μ_B for **1a-240**. The μ_{eff}/Co(300 K) value of fully dehydrated sample **1a-220** agrees well with the presence of high-spin octahedral Co^{II} with a significant orbital contribution.[10] Figure 1d shows the plot of the effective magnetic moments against dehydration temperature. The moment increases almost linearly with increasing dehydration temperature in the range of 120–220 °C. Apparently, the magnetic properties of **1a** can be tuned simply by thermal treatment at different temperatures. For comparison, the

[*] Dr. S.-S. Bao, Dr. Y.-H. Su, X. Liang, Prof. Dr. L.-M. Zheng
State Key Laboratory of Coordination Chemistry, Coordination Chemistry Institute, School of Chemistry and Chemical Engineering
Nanjing University, Nanjing 210093 (P. R. China)
Fax: (+86) 25-8331-4502
E-mail: lmzheng@nju.edu.cn
Dr. F.-C. Hu, Dr. Z. Sun, Prof. Dr. S. Wei
National Synchrotron Radiation Laboratory
University of Science and Technology of China
Hefei 230029 (P. R. China)
E-mail: sqwei@ustc.edu.cn
Dr. Y. Liao, Prof. Dr. J. Ma
Theoretical and Computational Chemistry Institute
School of Chemistry and Chemical Engineering
Nanjing University, Nanjing 210093 (P. R. China)
E-mail: majing@nju.edu.cn
Prof. Dr. R. Alberto
Institute of Inorganic Chemistry, University of Zurich
8057 Zurich (Switzerland)

[**] Financial supports by the NSF of China (No. 11079021, 20825312, 10725522, 21021062), NSF of Jiangsu Province (No. BK2009009), the National Basic Research Program of China (2007CB925102, 2010CB923402, 2011CB808600) are acknowledged. We thank Prof. N. Kobayashi for valuable discussions.

Supporting information for this article is available on the WWW under http://dx.doi.org/10.1002/anie.201007872.

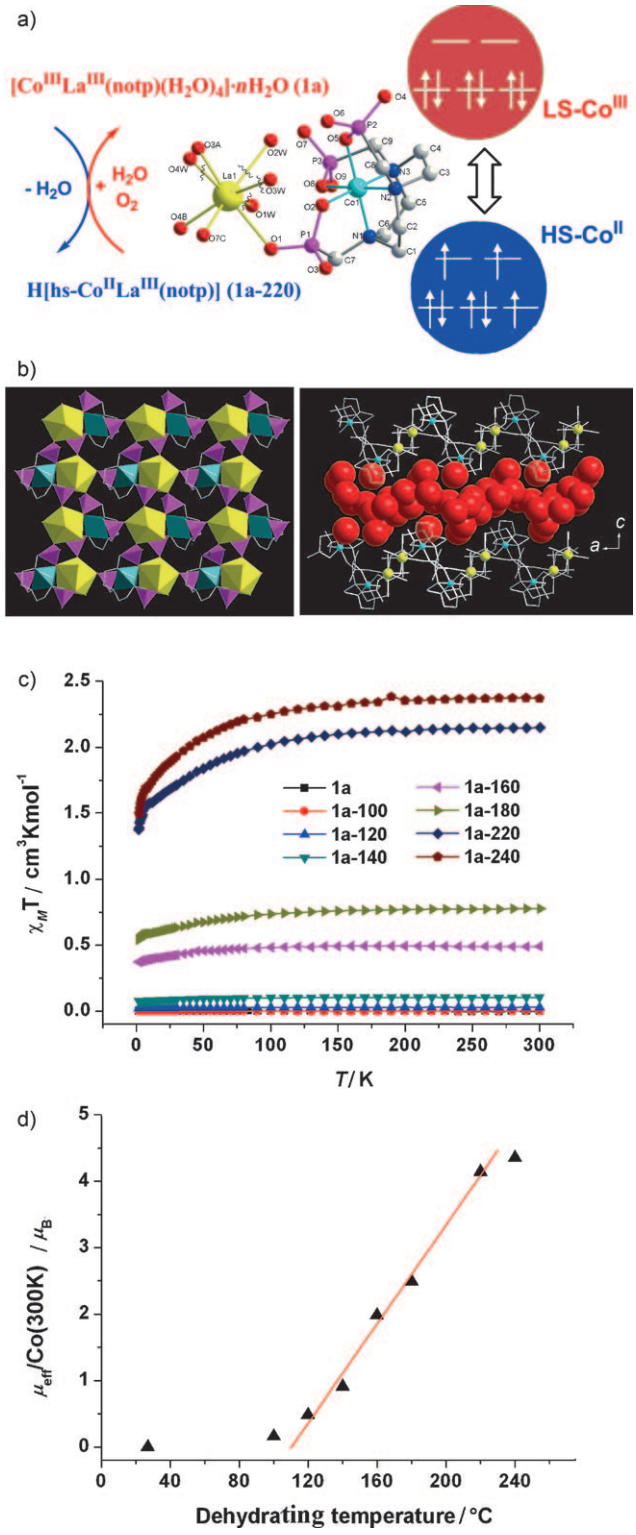

Figure 1. a) Scheme of the valence change between **1a** and **1a-220**. b) One layer and packing diagram of **1a** along the *b* axis. Color code: blue, Co; yellow, La; red O. c) $\chi_M T$ versus *T* plots for **1a** and samples dehydrated at 100, 120, 140, 160, 180, 220, and 240 °C for 1 h. d) μ_{eff}/Co(300 K) versus dehydrating temperature.

magnetic properties of the related mononuclear compound $[Co^{III}(notpH_3)]\cdot 3H_2O$ (**2a**) were also studied. Both **2a** and **2a-220** (thermally treated at 220 °C for 1 h) were found to be diamagnetic species.

To elucidate the origin of the change of the electronic structure of cobalt in **1a** on dehydration, UV/Vis spectra of solid-state samples of **1a** and **1a-220** were recorded, and time-dependent (TD) DFT[11] calculations on the structural units of **1a** and **1a-220** were carried out at the TD-B3LYP/SDD-6-311 + G** level (Figure 2). The calculated excitation energies

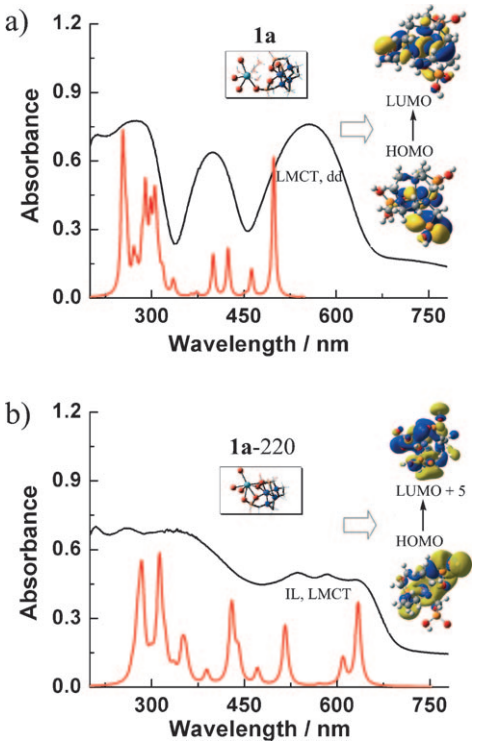

Figure 2. Absorption spectra of a) **1a** and b) **1a-220** obtained from experiments (black curves) and TD-DFT calculations (red curves). The theoretical absorption spectra were simulated by using a Lorentzian convolution with 30 nm half-widths.

of **1a** and **1a-220** correlate fairly well with experimental absorption spectra in the relative locations of the absorption peaks. The detailed results of the low-lying excitation wavelengths and the composition of frontier molecular orbitals involved in the transition are summarized in Table S3 of the Supporting Information. The low-energy transitions calculated for **1a** correspond to excitations from MOs formed mainly by 2p orbitals of O/P and 3d orbitals of Co ($3d_{xy}$, $3d_{yz}$ and $3d_{xz}$) into the $3d_{x^2-y^2}$ and $3d_{z^2}$ orbitals of Co. They can be characterized as mixed ligand-to-metal charge-transfer (LMCT) transitions with some d→d contributions. The TD-DFT calculations also predict predominant intraligand (IL) charge-transfer transition of the PO_3 ligand in **1a-220**.

If we exclude the ligand-to-metal transitions and mainly concentrate on the d→d transitions of Co, we can also resort to ligand-field theory to qualitatively evaluate the strength of the d→d transitions. Compound **1a** has bands at 17762 and 25063 cm^{-1}, assigned to the $^1A_{1g}\rightarrow{}^1T_{1g}$ (υ_1) and $^1A_{1g}\rightarrow{}^1T_{2g}$ (υ_2) d–d transitions of ls-Co^{III}, respectively. Accordingly, calculation of the ligand-field splitting parameter Δ_0 on the basis of

the d^6 Tanabe–Sugano diagram leads to a value of 19205 cm^{-1}. For **1a-220**, three bands are observed at about 8135, 17153, and 18657 cm^{-1}, assigned to d–d transitions $^4T_{1g}\rightarrow{}^4T_{2g}$ (υ_1), $^4T_{1g}\rightarrow{}^4A_{2g}$ (υ_2), and $^4T_{1g}\rightarrow{}^4T_{2g}(P)$ (υ_3) for hs-Co^{II}, respectively. The much smaller calculated Δ_0 for Co^{II} in **1a-220** (9131 cm^{-1}) favors a high-spin state. Clearly, the strong ligand field arising from the chelate effect stabilizes a low-spin state of Co^{III} in **1a**. On dehydration, the ligand field around the cobalt ion is weakened sufficiently to stabilize high-spin Co^{II}.

Extended X-ray absorption fine structure (EXAFS) spectroscopy provides information on coordination numbers and interatomic distances around the X-ray-absorbing atoms.[12] To investigate the change of the Co and La coordination sphere during the dehydration process, Co K-edge and La L_3-edge EXAFS measurements were conducted for **1a**, **1a-160**, **1a-180**, and **1a-220**. Figure 3a and b show Co K-edge k^3-weighted $\chi(k)$ data and their Fourier transforms (FT), respectively. The overall oscillation patterns of the $k^3\chi(k)$ functions for **1a**, **1a-160**, and **1a-180** are very similar, except for the gradually decreasing intensity with increasing dehydration temperature. They all show an FT peak at the same position of around 1.5 Å, corresponding to the nearest Co–O and Co–N coordination. For dehydrated complex **1a-220**, the $k^3\chi(k)$ pattern is distinctly different and, more importantly, the first FT peak is shifted significantly to the higher-R side of 1.7 Å and a shoulder on the low-R side is visible. The distinct spectroscopic features of **1a-220** with respect to the other samples indicate that the local atomic arrangements around Co ions have changed greatly. To reveal quantitatively this structural change, we performed curve fitting for the first FT peak in R space using Kaiser–Bessel windows by taking into account the Co–O and Co–N coordination pairs (Figure 3b). The extracted structural parameters are summarized in Table 1. For **1a**, the data fit leads to three nitrogen atoms at 1.92 Å and three oxygen atoms at 1.95 Å, which are close to those obtained by single-crystal structure determination (1.934 and 1.927 Å, respectively). The most interesting finding is that the Co–O bond length increases gradually while the Co–N bond length shrinks slightly with increasing dehydration temperature. Specifically, for **1a-220** a significantly elongated Co–O distance of 2.12 Å is observed, which is much longer than the Co–N bond length (1.88 Å). Hence, in combination with the UV/Vis spectra, the EXAFS results suggest that the elongated Co–O distances on dehydration may play an important role in changing the ligand-field strength and therefore mediating the spin state of the Co ions.

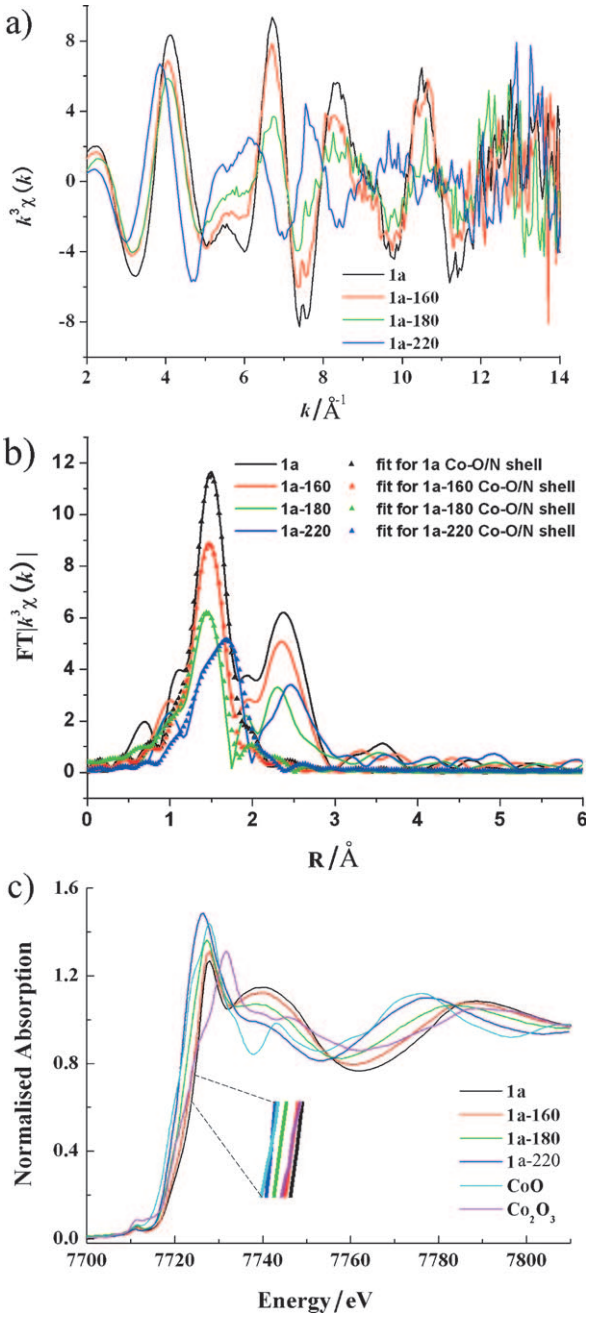

Figure 3. a) Co K-edge k^3-weighted EXAFS signals, b) Fourier-transformed space (R space) at Co K-edge, and c) Co K-edge XANES spectra of **1a**, **1a-160**, **1a-180**, **1a-220**, CoO, and Co_2O_3.

Table 1: Local structural fitting parameters of the Co–N and Co–O shells around Co in **1a**, **1a-160**, **1a-180**, and **1a-220**.

Sample	Shell	R [Å]	N	S_0^2	ΔE_0 [eV]	σ^2 [Å^2]
1a	Co–N	1.92(3)	3.00	1.00(0)	0.07(9)	0.0026(5)
	Co–O	1.95(3)	3.00	0.89(8)	2.21(5)	0.0030(2)
1a-160	Co–N	1.92(3)	3.00	1.00(0)	2.39(4)	0.0027(1)
	Co–O	1.98(3)	3.00	0.89(8)	2.21(5)	0.0030(2)
1a-180	Co–N	1.90(7)	3.00	1.00(0)	2.47(2)	0.0047(3)
	Co–O	2.00(5)	3.00	0.89(8)	2.91(6)	0.0079(7)
1a-220	Co–N	1.88(1)	3.00	1.00(0)	2.12(3)	0.0045(0)
	Co–O	2.12(2)	3.37	0.89(8)	0.50(0)	0.0035(0)

The Co K-edge X-ray absorption near edge structure (XANES) spectra of **1a**, **1a-160**, **1a-180**, and **1a-220** are shown in Figure 3c, which also displays the spectra of CoO and Co_2O_3 standards. Edge energy was previously used to qualitatively monitor changes in the oxidation state of cobalt. The edge position of **1a** of 7724 eV, obtained at half-height of the normalized edge jump, is identical to that of the Co_2O_3 standard and 3 eV higher than that of **1a-220** (7721 eV). The latter is identical to that of the CoO standard. The results

suggest that the Co oxidation state is 3+ in **1a** and 2+ in **1a-220**.[7b,13] For partially dehydrated samples **1a-160** and **1a-180**, the edge positions are 7723 and 7722 eV, respectively. Clearly, when the dehydration temperature increases, the edge position is shifted to a lower energy corresponding to a reduced effective charge of the cobalt ions. The pre-edge feature, originating from the 1s→3d transition, is observed at about 7711.3 eV for **1a** and about 7710.7 eV for **1a-220**, in agreement with those found in other octahedral Co^{III} and Co^{II} complexes, respectively.[14]

Furthermore, we investigated the La L_3-edge EXAFS data and found that the local structure features of La–O, such as coordination number and bond lengths, remain almost the same in **1a**, **1a-160**, **1a-180**, and **1a-220** (Table S8 and Figure S4, Supporting Information). Since four coordinated water molecules are removed from around an La atom on heating to 220 °C, the vacant sites of the lanthanide ion could be refilled by the neighboring oxygen atoms of the adjacent Co(notp) moieties. A careful analysis revealed that the closest uncoordinated La···O distances in **1a** are 3.521(4), 4.216(4), and 4.859(4) Å for La1···O2, La1···O5, and La1···O8, respectively. Since oxygen atoms O2, O5, and O8 also bind to the Co atom, coordination of these oxygen atoms to La would lead to elongation of the corresponding Co–O distances and thus affect the electronic configuration of the Co atom. Apparently, the driving force of the geometrical rearrangement in the cobalt coordination sphere of **1a** on dehydration is the variation around the La^{III} coordination sphere.

To rationalize the above experimental results, a DFT study was conducted. Because of the large radius of lanthanide ions, usually high coordination numbers are preferred, and some of the available coordination sites are often blocked by solvent molecules, such as water in our case. To simulate the geometrical variation during dehydration of lanthanum–cobalt compound **1a**, a cluster model including four building units (Scheme S1, Supporting Information) was selected from the crystal packing in such a way that the La–Co stoichiometry is retained. The DFT optimization revealed that a certain structural distortion occurs after removal of the water molecules, as shown in a single building block (Figure 2b). Three O atoms from adjacent $notp^{6-}$ ligand that directly chelate the Co atom are pulled toward the lanthanide ion to occupy the coordination sites vacated by water molecules. The variation around La^{III} subsequently leads to a geometrical rearrangement in the cobalt coordination sphere from nearly octahedral (**1a**) to distorted octahedral (**1a-220**), and hence changes its electronic structure.

Within the unrestricted single-determinant approach (at both the UB3LYP and UBHandHLYP levels), the singlet state is confirmed to be the most stable electronic state for hydrated compound **1a**, while dehydrated **1a-220** has a ground quintet spin state with the spin density mostly localized on the cobalt atom. An NBO analysis revealed that cobalt switches from low-spin to high-spin during the course of dehydration, with concomitant slight increase (0.3e) in the population of 3d electrons.

In conclusion, diamagnetic layered compound $[Co^{III}La^{III}(notp)(H_2O)_4]\cdot n\,H_2O$ (**1a**) can undergo thermally induced electron transfer through gradual release of the coordinated water molecules around the La atom. Thus, the magnetic properties of this compound can be modulated in a controllable manner by means of thermal treatment in the range 120–220 °C. More interestingly, the dehydrated high-spin $H[hs\text{-}Co^{II}La^{III}(notp)]$ (**1a-220**) can turn back into low-spin $[ls\text{-}Co^{III}La^{III}(notp)(H_2O)_4]\cdot n\,H_2O$ (**1a**) on rehydration in air. However, one question remains open: reduction of Co^{III} should lead to oxidation of another species. The oxidized species could be either the coordinated water or the organic ligand. Preliminary cyclic voltammetry results show that the reduction potential from Co^{III} to Co^{II} in compound **1a** is −0.37 V (vs. Ag/AgCl). The redox process is irreversible, possibly due to the electronic and structural rearrangement.[15] Further work is in progress to understand the mechanism of the process.

Experimental Section

$[Co^{III}La^{III}(notp)(H_2O)_4]\cdot n\,H_2O$ (**1a**) was synthesized by hydrothermal treatment of a mixture of $[La^{III}(notpH_4)(NO_3)(H_2O)]\cdot 4\,H_2O$[16] (0.05 mmol, 0.035 g) and $Co(NO_3)_2\cdot 6\,H_2O$ (0.20 mmol, 0.071 g) in water (8 mL) at 120 °C for 48 h. Purple quadrangular sheetlike crystals were obtained as a monophasic material in a yield of 50% (based on La). Elemental analysis calcd (%) for $C_9H_{26}N_3O_{13}P_3CoLa\cdot 5\,H_2O$: C 14.13, H 4.74, N 5.49; found: C 14.07, H 5.12, N 5.47; IR (KBr): $\tilde{\nu}$ = 3395(br), 1654(m), 1460(w), 1281(w), 1253(w), 1134(s), 1098(w), 1069(w), 1048(s), 1011(w), 993(w), 943(w), 779(w), 611(m), 491 cm^{-1} (w); TGA: 21.2% (50–220 °C, calcd 21.1%).

$[Co^{III}(notpH_3)]\cdot 3\,H_2O$ (**2a**) was obtained as purple block crystals in 87% yield by diffusion of methanol into an aqueous solution of $Co(NO_3)_2\cdot 6\,H_2O$ (0.10 mmol, 0.035 g) and $notpH_6$ (0.10 mmol, 0.041 g). Elemental analysis calcd (%) for $C_9H_{21}N_3O_9P_3Co\cdot 3\,H_2O$: C 20.74, H 5.22, N 8.06; found: C 20.66, H 5.19, N 8.12; IR (KBr): $\tilde{\nu}$ = 3454(br), 1655(m), 1491(w), 1460(w), 1283(w), 1254(w), 1128(s), 1099(m), 1072(s), 1049(s), 999(w), 951(w), 931(w), 802(w), 775(w), 609(m), 497 cm^{-1} (m); ESI-MS: *m/z*: 468.08 $[Co^{III}(notpH_4)]^+$; TGA: 10.3% (30–140 °C, calcd. 10.4%).

Received: December 14, 2010
Revised: March 15, 2011
Published online: May 9, 2011

Keywords: cobalt · heterometallic complexes · lanthanum · magnetic properties · N,O ligands

[1] a) S. Kitagawa, R. Kitaura, S. Noro, *Angew. Chem.* **2004**, *116*, 2388–2430; *Angew. Chem. Int. Ed.* **2004**, *43*, 2334–2375; b) O. Sato, J. Tao, Y.-Z. Zhang, *Angew. Chem.* **2007**, *119*, 2200–2236; *Angew. Chem. Int. Ed.* **2007**, *46*, 2152–2187; c) E. Neuscamman, S. Flores-Torres, P. S. Cornaglia, A. A. Aligia, C. A. Balseiro, G. K.-L. Chan, H. D. Abruña, D. C. Ralph, *Science* **2010**, *328*, 1370–1373.

[2] a) G. J. Halder, C. J. Kepert, B. Moubaraki, K. S. Murray, J. D. Cashion, *Science* **2002**, *298*, 1762–1765; b) M. Nihei, L. Han, H. Oshio, *J. Am. Chem. Soc.* **2007**, *129*, 5312–5313; c) K. S. Min, A. G. DiPasquale, A. L. Rheingold, H. S. White, J. S. Miller, *J. Am. Chem. Soc.* **2009**, *131*, 6229–6236; d) Z. Ni, M. P. Shores, *J. Am. Chem. Soc.* **2009**, *131*, 32–33; e) A. Bousseksou, G. Molnar, J. A. Real, K. Tanaka, *Coord. Chem. Rev.* **2007**, *251*, 1822–1833; f) L. Zhang, G.-C. Xu, H.-B. Xu, T. Zhang, Z.-M. Wang, M. Yuan, S. Gao, *Chem. Commun.* **2010**, *46*, 2554–2556.

[3] a) M. Ohba, W. Kaneko, S. Kitagawa, T. Maeda, M. Mito, *J. Am. Chem. Soc.* **2008**, *130*, 4475 – 4484; b) E. Coronado, M. C. Gimenez-Lopez, T. Korzeniak, G. Levchenko, F. M. Romero, A. Segura, V. Garcia-Baonza, J. C. Cezar, F. M. F. de Groot, A. Milner, M. Paz-Pasternak, *J. Am. Chem. Soc.* **2008**, *130*, 15519 – 15532; c) E. Coronado, M. C. Gimenez-Lopez, G. Levchenko, F. M. Romero, V. Garcia-Baonza, A. Milner, M. Paz-Pasternak, *J. Am. Chem. Soc.* **2005**, *127*, 4580 – 4581.

[4] a) D. E. Freedman, D. M. Jenkins, A. T. Iavarone, J. R. Long, *J. Am. Chem. Soc.* **2008**, *130*, 2884 – 2885; b) T. Mahfoud, G. Molnar, S. Bonhommeau, S. Cobo, L. Salmon, P. Demont, H. Tokoro, S.-I. Ohkoshi, K. Boukheddaden, A. Bousseksou, *J. Am. Chem. Soc.* **2009**, *131*, 15049 – 15054.

[5] a) R. M. Buchanan, C. G. Pierpont, *J. Am. Chem. Soc.* **1980**, *102,* 4951 – 4957; b) D. M. Adams, A. Dei, A. L. Rheingold, D. N. Hendrickson, *J. Am. Chem. Soc.* **1993**, *115*, 8221 – 8229; c) P. Gütlich, A. Dei, *Angew. Chem.* **1997**, *109*, 2852 – 2855; *Angew. Chem. Int. Ed. Engl.* **1997**, *36*, 2734 – 2736; d) A. Dei, D. Gatteschi, C. Sangregorio, L. Sorace, *Acc. Chem. Res.* **2004**, *37*, 827 – 835; e) C. G. Pierpont, *Coord. Chem. Rev.* **2001**, *216–217*, 99 – 125; f) E. Evangelio, D. Ruiz-Molina, *C. R. Chim.* **2008**, *11*, 1137 – 1154; g) O. Sato, A. Cui, R. Matsuda, J. Tao, S. Hayami, *Acc. Chem. Res.* **2007**, *40*, 361 – 369.

[6] a) D. Kiriya, H. C. Chang, S. Kitagawa, *J. Am. Chem. Soc.* **2008**, *130*, 5515 – 5522; b) J. S. Miller, K. S. Min, *Angew. Chem.* **2009**, *121*, 268 – 278; *Angew. Chem. Int. Ed.* **2009**, *48*, 262 – 272; c) R. D. Schmidt, D. A. Shultz, J. D. Martin, P. D. Boyle, *J. Am. Chem. Soc.* **2010**, *132*, 6261 – 6273; d) G. Poneti, M. Mannini, L. Sorace, P. Sainctavit, M.-A. Arrio, E. Otero, J. C. Cezar, A. Dei, *Angew. Chem.* **2010**, *122*, 1998 – 2001; *Angew. Chem. Int. Ed.* **2010**, *49*, 1954 – 1957.

[7] a) O. Sato, T. Iyoda, A. Fujishima, K. Hashimoto, *Science* **1996**, *272*, 704 – 705; b) A. Bleuzen, C. Lomenech, V. Escax, F. Villain, F. Varret, C. Cartier dit Moulin, M. Verdaguer, *J. Am. Chem. Soc.* **2000**, *122*, 6648 – 6652; c) C. P. Berlinguette, A. Dragulescu-Andrasi, A. Sieber, H. U. Gudel, C. Achim, K. R. Dunbar, *J. Am. Chem. Soc.* **2005**, *127*, 6766 – 6799; d) Y.-Z. Zhang, D.-F. Li, R. Clérac, M. Kalisz, C. Mathonière, S. M. Holmes, *Angew. Chem.* **2010**, *122*, 3840 – 3844; *Angew. Chem. Int. Ed.* **2010**, *49*, 3752 – 3756; e) C. Avendano, M. G. Hilfiger, A. Prosvirin, C. Sanders, D. Stepien, K. R. Dunbar, *J. Am. Chem. Soc.* **2010**, *132*, 13123 – 13125; f) J.-D. Cafun, G. Champion, M.-A. Arrio, C. C. dit Moulin, A. Bleuzen, *J. Am. Chem. Soc.* **2010**, *132*, 11552 – 11559.

[8] a) A. Clearfield, *Prog. Inorg. Chem.* **1998**, *47*, 371 – 510; b) Y.-S. Ma, H. Li, J.-J. Wang, S.-S. Bao, R. Cao, Y.-Z. Li, J. Ma, L.-M. Zheng, *Chem. Eur. J.* **2007**, *13*, 4759 – 4769; c) Y.-S. Ma, Y. Song, L.-M. Zheng, *Inorg. Chim. Acta* **2008**, *361*, 1363 – 1371.

[9] Crystal data for **1a**: Monoclinic, $P2_1/c$, $a = 9.2220(19)$, $b = 11.407(2)$, $c = 28.062(6)$ Å, $\beta = 95.600(4)°$, $V = 2937.9(10)$ Å^3, $Z = 4$, $F(000) = 1456$, $\rho_{calcd} = 1.648\ g\,cm^{-3}$, $\mu(Mo_{K\alpha}) = 2.225\ mm^{-1}$ ($\lambda = 0.71073$ Å), $R_1 = 0.0639$, $wR_2 = 0.1196$, GooF = 1.016. CCDC 804469 contains the supplementary crystallographic data for this paper. These data can be obtained free of charge from The Cambridge Crystallographic Data Centre via www.ccdc.cam.ac.uk/data_request/cif.

[10] O. Kahn, *Molecular Magnetism*, VCH, New York, **1993**.

[11] M. K. Casida, C. Jamorski, K. C. Casida, D. R. Salahub, *J. Chem. Phys.* **1998**, *108*, 4439 – 4449.

[12] D. C. Koningsberger, R. Prins, *X-ray Absorption: Principle, Applications, Techniques of EXAFS, SEXAFS and XANES*, Wiley, New York, **1988**.

[13] M. Risch, V. Khare, I. Zaharieva, L. Gerencser, P. Chernev, H. Dau, *J. Am. Chem. Soc.* **2009**, *131*, 6936 – 6937.

[14] a) P. D. Bonnitcha, M. D. Hall, C. K. Underwood, G. J. Foran, M. Zhang, P. J. Beale, T. W. Hambley, *J. Inorg. Biochem.* **2006**, *100*, 963 – 971; b) M. Sano, *Inorg. Chem.* **1988**, *27*, 4249 – 4253; c) J. Y. Chang, B. N. Lin, Y. Y. Hsu, H. C. Ku, *Physica B* **2003**, *329–333*, 826 – 828.

[15] F. B. Johansson, A. D. Bond, U. G. Nielsen, B. Moubaraki, K. S. Murray, K. J. Berry, J. A. Larrabee, C. J. McKenzie, *Inorg. Chem.* **2008**, *47*, 5079 – 5092.

[16] S.-S. Bao, L.-F. Ma, Y. Wang, L. Fang, C.-J. Zhu, Y.-Z. Li, L.-M. Zheng, *Chem. Eur. J.* **2007**, *13*, 2333 – 2343.

